NbTi and Nb_3Sn Superconducting Undulator Designs

S. Prestemon, D. Dietderich, S. Marks, R. Schlueter

Lawrence Berkeley Laboratory, USA

Abstract. Superconducting undulator performance is a function of a number of accelerator -specific parameters. Two very important parameters are the allowable vacuum gap and beam heating, e.g. RF and synchrotron radiation. We evaluate theoretical performance for planar superconducting undulator designs cooled with existing cryocooler technology as a function of gap, beam-heating, and cryocooler performance, for two existing low-temperature superconductors, NbTi and Nb_3Sn. Optimal superconducting undulator performance depends critically on both magnetics design and operating conditions. Regimes where a cold-bore vacuum chamber cryogenics design is preferable and those where an intermediate-temperature design may yield superior performance are quantified.

INTRODUCTION

Superconducting magnets are steadily gaining acceptance in accelerator rings. Early devices were typically wavelength shifters and wigglers [1]. More recently, bend magnets have been incorporated in the ring lattice, a clear sign of the acceptance of superconducting technology in accelerators [2]. Currently much effort is being devoted to the development of superconducting undulators (SCU's), particularly for "short-period" devices, e.g. less than ~30mm periods. SCU's can provide higher fields at a given period, providing users with expanded spectral range, with good overlap of harmonics.

The anticipated performance of an SCU depends strongly on 1) the properties of the superconductor and details of the coilpack, 2) the design parameters, such as coilpack dimensions and device period and gap, 3) heat sources and cryogenic design, and 4) field quality and phase-error minimization. In this paper we will concentrate on the first three issues, in particular the relation between anticipated performance and imposed heat load.

NbTi AND Nb_3Sn SUPERCONDUCTORS

Superconductors have evolved at a rapid pace over the last couple of decades. Here we concentrate on NbTi and Nb_3Sn conductors, which are the most readily available and are mature technologies. We begin by presenting critical current (J_c) data for example conductors. We then discuss other issues that must be considered in the selection of conductor, and their impact on performance.

The critical current of NbTi and Nb_3Sn, both type II superconductors, is typically modeled by considering the effects of field, temperature, and strain, using critical-state theory to estimate the pinning force [3, 4, 5, 6]. Examples of Jc data for measured conductors are presented in Table 1. Note that significant advancements are being made in the critical current for Nb_3Sn, motivated largely by high-energy physics applications [7].

TABLE 1. Examples of superconductor performance. Values are for 4.2K.

Material	Jc (12 T) A/mm2	Jc (6T) A/mm2	Comments
Nb_3Sn, OST RRP 6555 [8]	~3100	~8900	Strand for LBNL HD-1 dipole prototype
Nb_3Sn, OST ORe 143c	~2400	~7100	Strand for LBNL RD-3c dipole prototype [9]
Nb_3Sn, OST ORe 0021B14B	~2000	~6000	Used in LBNL SCU prototype
NbTi, Industrial sampling (Lee, 2002)	-	~2100	Available in long lengths
NbTi, APC, Heussner et al. (UW-ASC) [10]	-	~2900	R&D effort, high Cu:SC

The actual performance of a device is governed by the average current density, which is a function of the critical current, but also of the copper fraction (critical for stability and protection), the insulation thickness, and void space. Due to the small dimensions associated with short-period SCU's, resulting in small bend radii and large bending strain, a wind-and-react approach must be used with Nb_3Sn. The heat treatment, reaching ~650C or more, rules out most insulation materials. The most common approach is to insulate with S-glass fibers, which typically results in an insulation thickness of about 50 microns. NbTi is usually insulated with formvar with a thickness of about 25 microns.

The choice of copper fraction must be based on concerns for stability of the conductor at the design current and protection of the magnet during a quench. The relatively low stored energy of a SCU (typically ~1kJ/period or less) suggests that high copper current densities, and hence low copper fractions, may be tolerable. We are currently investigating the limits of magnet protection with a 6-period prototype device that is designed to approach 6000 A/mm2 in the copper during a quench [11]. The Cu:SC ratio for NbTi is typically greater than one due in part to manufacturing issues. For Nb_3Sn, lower copper fractions are possible, provided protection can be accommodated. A coilpack cross-section with Asc/Atot~0.27 can be considered very good for a Nb_3Sn conductor, whereas a NbTi based design may be capable of slightly higher superconductor fraction due to thinner insulation.

PERFORMANCE CURVES FOR SUPERCONDUCTING UNDULATORS

The critical current and realistic assumptions about engineering current densities described above have been used to evaluate the performance of optimal undulator designs, as described in [11]. Figure 1 shows the effect of temperature on the critical current density for typical Nb_3Sn and NbTi conductors, and the impact of the temperature dependence on anticipated performance of Nb_3Sn based devices.

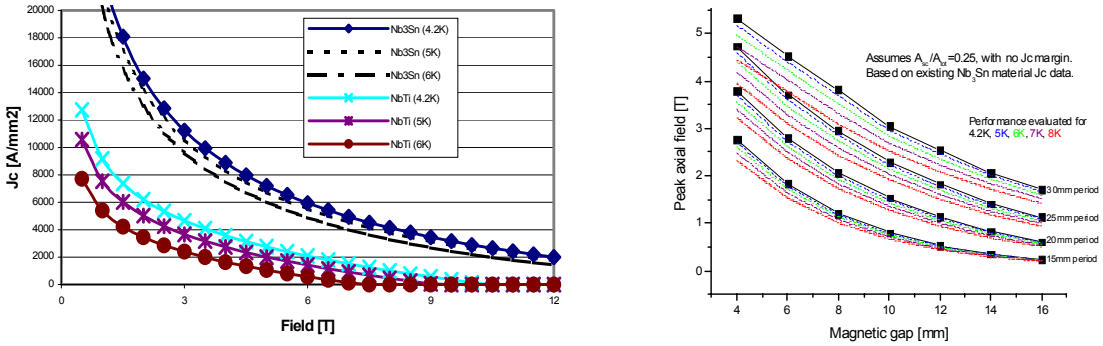

Figure 1. Example Jc curves for NbTi and Nb_3Sn at 4.2K, 5K, and 6K (left), and estimated performance curves for Nb_3Sn – based undulators at different gaps and for different temperatures, assuming 25% superconductor area (right).

THERMAL LOADS AND CRYOCOOLER CAPACITY

The heat loads on an SCU include the usual conduction loads (Q_{static}), stemming from support structures and current leads, and radiation loads, from cryostat surfaces. Furthermore, there may be heat loads associated with the beam vacuum chamber and the beam itself. Although there are a number of potential heat loads associated with electron beams, the most important appear to be synchrotron radiation and image current heating (Q_{im}). Synchrotron radiation impinging on the vacuum chamber wall can easily lead to heat loads far in excess of any realistic cryostat design, and must be largely masked.

The image current heating at room temperature is a function of the surface resistivity ρ. At low temperatures and sufficiently high frequencies, the skin-depth δ_{skin} and mean free path of the electrons, λ_e, are of the same order of magnitude, and the anomalous skin effect negates the effective decrease in resistivity with temperature [12, 13]. For 4.2K operation in typical synchrotron ring scenarios, the power loss per unit length [14] is of the form

$$Q_{im} = \alpha \frac{I^2 l_S}{h(l_b)^{5/3}} Z_0^{2/3} (\rho \lambda_e)^{1/3} \qquad (1)$$

Here l_s is the bunch spacing, l_b is the bunch length, h is the half-gap, Z_0 is the free-space impedance, and α is a constant, based solely on the vacuum chamber geometry. Note that the power loss in this regime (extreme anomalous skin effect) is a function of the temperature-independent material parameter $\rho\lambda_e$, and no longer varies with the $\rho_{300K}/\rho_{4.2K}$ value of the material. Estimates of the $\rho\lambda_e$ value for different materials are shown in Table 2. Due to the 1/3 power dependence (see equation 1) and the rather small variation between materials, the selection of vacuum chamber material for cold-bore operation should be made based on mechanical and fabrication concerns. For the ALS, the heating predicted by equation (1) for a 4.2K vacuum wall is ~0.4 W/m under current operating conditions, and may reach ~2.6 W/m with future upgrades.

Most accelerator rings do not have cryogenic liquefiers available for cooling superconducting devices, and cryocooler based systems are of great interest [15]. Cryocooler designs can be classified in three categories: 1) they can be cryogen-free, with the cold-head cooling the device via conduction; 2) the system can be immersed in liquid helium, with the cold head conduction cooling the magnet, but the liquid available for continued operation in the case of a cryocooler malfunction (the cryogens also serve to decrease the initial cooldown time); 3) the cryocooler can be used as a recondensor, decoupling the cold head mechanically from the device [16]. In the latter case, care must be taken to minimize losses in the recondenser.

For operation below ~25K, two-stage cryocoolers must be considered. In the low temperature range of 4.2-10K, it is reasonable to assume that T(Q), where T is the cold-head temperature, is roughly linear [17]; the Sumitomo RDK415D device, for example, is nominally capable of extracting 1.5W at 4.2K, and 10W at 8.1K.

TABLE 2 Material properties associated with the extreme anomalous skin effect [18].

	Cu	Al	Ag	Au
300K resistivity (ρ) [Ohm-m]	1.74E-08	2.68E-08	1.59E-08	2.46E-08
ρλ [Ohm-m^2]	6.5187E-16	3.97E-16	8.43E-16	8.35E-16

COLD AND INTERMEDIATE TEMPERATURE VACUUM CHAMBER DESIGNS

The data presented in the previous sections suggests 1) that cold-bore operation at T>4.2K should be considered when using Nb_3Sn and cryocoolers, and 2) that under some operating conditions better performance (higher B) may be achieved by incorporating an intermediate temperature (~20K) vacuum chamber or liner. The two limiting cases are 1) rings with negligible image-current heating, where performance will be enhanced by cold-bore operation, and 2) rings with significant image current heating, requiring an intermediate temperature intercept. Many existing synchrotron rings appear to operate in an intermediate regime, where image current heating and traditional heat loads are roughly of the same order. In order to compare cold bore and intermediate-temperature designs, we assume the following functional dependencies (basic functional relations are shown on the left; models used for calculations are shown on the right):

$$Q_{cold} = f(Q_{static}, Q_{im}(g_v), type) \qquad Q_{static} + Q_{im}(g_v) = Q_{static} + Q_0 h_0/(h-\Delta h);\ \ h = g_v/2 \tag{2}$$

$$T_{cold} = f(Q_{cold}) \qquad T_{cold} = T_0 + aQ_{cold} \tag{3}$$

$$g_m = f(g_v, type) \qquad g_m = g_v + \Delta g \tag{4}$$

$$J_c = f(T_{cold}, B_{coil}) \tag{5}$$

$$B = f(g_m, J_c) \tag{6}$$

The dependence on *type* in equations (2) and (4) refers to cold or intermediate temperature vacuum chamber operation. In equation (2), Q_0 is determined from equation (1), with h_0 a reference half-gap, and Δh is the estimated beam trajectory offset. T_0 is the zero-load cold-head temperature, a is the slope of the cryocooler cold head performance curve, and B is the field in the gap. The vacuum chamber wall thickness is $\Delta g/2$. Equations (5) and (6) are solved using the optimal load-line methodology described in [11]. Figure 2 presents calculated performance curves based on operation at temperatures above 4.2K, assuming a gap-dependent heat load as described by equations (2-6). The heat load is a strong function of the ring-dependent parameters, modeled here by the parameter Q_0. Performance with aggressive (GM) and conservative (PT) assumed cooling slopes (a) are shown.

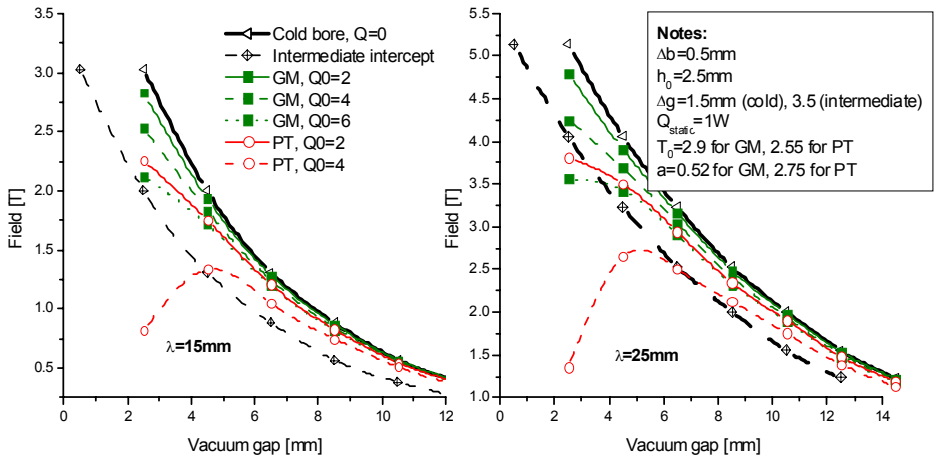

FIGURE 2. Plots of calculated performance for 15mm period (left) and 25mm period (right) Nb_3Sn-based undulators, assuming a gap-dependent heat-load variation as described in equations (2-6). Parameter values are provided in the note on the graph.

CONCLUSIONS

The temperature-dependent behavior of J_c for NbTi and Nb_3Sn has been reviewed. Nb3Sn has superior performance compared to that of NbTi at all temperatures, specifically both at 4.2K and higher. For operating conditions with low beam-heat loads a cold-bore Nb3Sn design yields best performance. Furthermore, unlike NbTi, Nb3Sn retains significant J_c for temperatures of 10K or higher, making operation at such temperatures of interest for cryocooler-based systems when beam heat loads are expected. For high heat load scenarios, the more robust intercept temperature designs (either NbTi or Nb_3Sn) should be considered. The attainable field performance is also strongly dependent on the cold-head temperature of the cooling unit as a function of applied load.

ACKNOWLEDGMENTS

This work was supported by the Director, Office of Science, of the US Department of Energy under Contract No. DE-AC03-76SF00098.

REFERENCES

1. Mezentsev, N., ESRF Workshop on Superconducting Undulators, June, 2003.
2. Zbasnik, J., et al., IEEE Trans. On applied Superconductivity, Vol 11, N0 1, March, 2001, pp2531-2534
3. Godeke, A., Ten Haken, B., and H.J. Ten Kate, H., IEEE Trans. on Applied Superconductivity, Vol. 9, No.2, June 1999
4. Ten Haken, B., Godeke, A. and H. J. Ten Kate, H., Journal of Applied Physics, Vol. 85, No. 6, March 1999
5. Green, M. A., IEEE Trans. on Magnetics, 25 (2), 1989.
6. Summers, L. T., et al., IEEE Trans. on Magnetics, 27(2), p. 2041, 1991.
7. Scanlan, R. M., Dietderich, D. R., Transactions on Applied Superconductivity, Vol. 13, No. 2, p15-36, June 2003.
8. Lietzke, A., et al., IEEE Trans. Appl. Super. vol. 13 (2) June 2003, p3470-3473.
9. Parrell, J., et al., IEEE Trans. Appl. Super. vol. 13 (2) June 2003, p1292-1296.
10. Heussner, R. W., Marquardt, J. D., Lee, P. J., and Larbalestier, D. C., Applied Physics letters, 70(7), February 1997
11. Prestemon, S. et al., Proceedings, PAC2003.
12. Landau and Lifschitz, Vol. X, "Physical Kinetics", Ed. Pitaevskii, L. P., Pergamon Press, Nov. 1981.
13. Caspers, F., Morvillo, M., Ruggiero, F. and Tan, J., LHC Project Report 307, CERN, August 1999.
14. Podobedov, B., ESRF Workshop on Superconducting Undulators, June, 2003.
15. Van Sciver, S. W., Physica C, 354, p.129-135, 2001.
16. Taylor, C. E., Engineering Note SC MAG 759, Lawrence Berkeley National Laboratory, January, 2002.
17. Green, M. A., paper to be presented at CEC-ICMC, 2003.

18. Kittel, C. “Introduction to Solid State Physics”, 5th Ed., John Wiley and Sons, 1976.